Ring-shaped deposition patterns in small nozzle-to-plate distance impactors

S. Fredericks & J. R. Saylor

Taylor & Francis
Taylor & Francis Group

Ring-shaped deposition patterns in small nozzle-to-plate distance impactors

S. Fredericks and J. R. Saylor

Department of Mechanical Engineering, Clemson University, Clemson, SC, USA

ABSTRACT

Experiments were carried out in an impactor, where the distance between the impactor nozzle and the impactor plate was small, much less than one nozzle diameter in separation. The aerosol deposition patterns in this impactor were investigated for aerosols in the 3–15 μm diameter range. Ring-shaped deposition patterns were observed where the internal diameter and thickness of the rings were a function of the particle diameter. Specifically, the inner diameter and ring thickness were correlated to the Stokes number, Stk; the ring diameter decreased with Stk, and the ring thickness increased with Stk. At $Stk \sim 0.4$ the ring closed up, leaving a mostly uniform disk deposition pattern. These ring patterns do not appear to correspond to patterns previously described in the literature, and an order of magnitude analysis shows that this is an inertially dominated process.

1. Introduction

Aerosols have significant health (Schwartz and Dockery 1992; Schwartz 1994; Pope et al. 1995; Davis et al. 2002; Schwartz et al. 2002; Seaton et al. 1995; Docker and Pope 1994) and environmental (Pruppacher and Klett 1978; Horvath 1993; Ramanathan et al. 2001; Kanakidou et al. 2005) effects whose magnitude depends on, among other things, the size and number density of these aerosols. It is therefore critical to have accurate and robust methods for measuring the aerosol size distribution. A commonly used instrument for this purpose is the impactor (Hinds 1982; Vincent 2007; Liu 1975; Marple 2004) which operates by accelerating an aerosol-laden flow through a nozzle onto a plate-oriented normal to the nozzle axis. This setup results in a low-diameter band-pass filter since large particles will deposit on the plate due to their inertia, while small particles pass around the impaction plate without deposition. By combining several of these plates, or stages, in series, an impactor cascade is created where each subsequent stage captures progressively smaller particle diameters. The particle size distribution can then be determined by gravimetrically measuring the mass deposited on the plate of each stage, with the number of bins in the resulting distribution equal to the number of stages in the cascade. Typical cascades have from five to eight stages, though impactors with more stages do exist such as the Sierra TAG, the MOUDI, nano-MOUDI, and the ELPI impactors which have 9, 10, 13,

and 13 stages, respectively. (Marple and Willeke 1976; Marple et al. 1991; Marple 2004; Marjamäki et al. 2000).

Impactor stages are typically characterized by their cutoff diameter, d_{50}, which is defined as the particle diameter for which 50% of the sampled particles will deposit on the impactor plate. The plot of the fraction of particles collected, η, versus particle diameter d is typically sigmoidal in shape, quickly approaching zero to the left of d_{50}, and quickly approaching unity to the right of d_{50}. The steeper this curve at d_{50}, the less uncertainty there is in the diameter range collected by each impactor stage (Arffman et al. 2011; Chen et al. 2011). The steepness of the sigmoidal collection curve is determined by the characteristics of the flow through the impactor stage, and is primarily controlled by the ratio of the distance between the impaction plate and the nozzle, S, and the nozzle diameter, W. Typically, impactor stages are designed to have $S/W > 1$ to maximize the steepness of the deposition curve. This is likely the reason that exploration of small S/W impactors has been minimal. It has been shown that by decreasing S/W, the steepness of the deposition curve decreases, collecting more particles below d_{50} and fewer particles above d_{50} than is the case for $S/W > 1$. Decreasing S/W also decreases d_{50} (Grinshpun et al. 2005; Marple and Willeke 1976; Liu 1975; Marple et al. 1974).

In an unrelated experiment, the authors used small S/W impactors. The goal in that work was to capture monodisperse particles for subsequent sizing via microscope

---

imaging. Because the particles were monodisperse, the steepness of the η versus d curve was not relevant. The resulting deposition patterns were unexpectedly ring shaped. The goal of the present work is to further explore these small S/W impactors. Specifically, we sought to determine if the ring-shaped patterns were robust and to find whether the geometry of the ring patterns were determined by impactor parameters.

2. Experimental method

Experiments were conducted at small S/W for a range of particle diameters to determine if any dimensional characteristics of the rings might be a function of particle diameter. The apparatus used to do this is shown in Fig. 1. The particles used in these experiments were composed of disodium fluorescein which were generated using a vibrating orifice aerosol generator (VOAG, TSI Model 3450). The disodium fluorescein was dissolved in a 50/50 water/isopropyl alcohol solvent. This solution was flowed through the VOAG, creating a monodisperse distribution of drops. Upon evaporation of the solvent, a monodisperse particle distribution remained having a diameter, d, determined by

$$d = \left(\frac{6QC}{\pi f}\right)^{\frac{1}{3}} \tag{1}$$

where C is the solution concentration, Q is the solution flowrate, and f is the vibration frequency of the VOAG orifice (Berglund and Liu 1973). Disodium fluorescein was used since it is a bright green dye which is easily visualized.

As shown in Fig. 1, the aerosol stream was convected from the VOAG through a vertically oriented drying column having a diameter of 100 mm using house air. The house air passed through a Kr-85 source (TSI Model 3077A), so that all of the air used in the jet was subjected to charge elimination. The house air had a relative humidity that was typically 5% and which facilitated evaporation
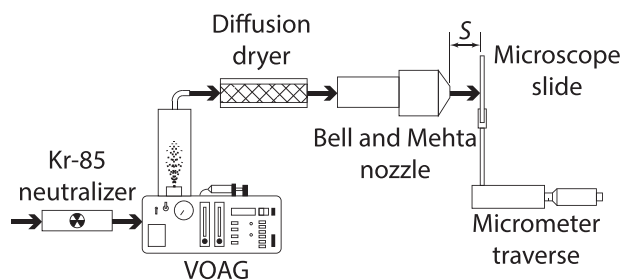

Figure 1. Apparatus used to generate monodisperse disodium fluorescein particles and measure the resulting deposition pattern.
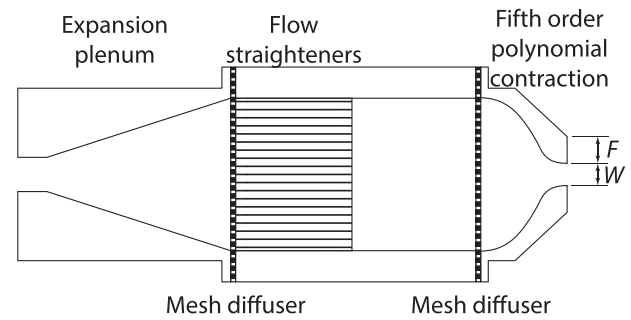

Figure 2. Schematic of the Bell and Mehta (1988) nozzle used to produce a uniform velocity jet. The diagram is not to scale.

of the solvent to create particles. The particles were flowed through a diffusion drier (ATI Model DD250) to ensure that they were fully dry and had a density, ρ, equal to that of pure disodium fluorescein and a diameter predicted by Eq. (1). The dry particles were then passed through a nozzle with an exit diameter, W, of 12.7 mm. As shown in Fig. 2 this nozzle consisted of three stages, an expansion plenum, followed by a flow straightener comprising packed 3 mm straws approximately 30 mm in length in a 50 mm straight plenum, and then the nozzle whose profile conformed to a fifth-order polynomial defined by Bell and Mehta (1988). Wire mesh diffusers with a mesh size of $\sim$ 0.5 mm were installed between each stage. The region surrounding the nozzle orifice had a flat face indicated as F in Fig. 2, and which was 2 mm wide. This nozzle is designed to provide a flat velocity profile at its exit. The jet exit velocity, U, was measured with a hand held anemometer (TSI Velocicalc).

A microscope slide mounted on a precision translation stage served as the impactor plate. As particle bounce was a concern, a sticky coating was applied to the microscope slide to aid in particle retention (Tsai et al. 2012; Pak et al. 1992; Turner and Hering 1987). This coating was created by pretreating the slide with a solution of Vaseline brand petroleum jelly dissolved in heptane at a 1:20 volume ratio in a method similar to that used by Sethi and John (1993). The microscope slide was dipped in this solution and then allowed to dry, resulting in a $\sim$ 4 μm thick film of petroleum jelly coating the microscope slide. The spacing between the nozzle and the slide, S, was set to 0.6 mm using the micrometer traverse, giving $S/W = 0.047$. The coated microscope slide was exposed to the aerosol laden jet for a period of time sufficient to allow a visible accumulation of particles on the slide. This duration ranged from 30 s to 5 min depending on the particle number density in the jet.

Attempts were made to confirm the particle diameter predicted by Eq. (1) by imaging the particles deposited on the slide at 10x using a microscope (Leica DM750) with a mounted digital camera (Cannon Rebel T3).

However, due to humidity in the laboratory the deposited fluorescein particles, which are very hygroscopic, would begin to absorb water from the laboratory air almost instantly upon removal of the microscope slide from the dry jet air. This would cause the particles to "melt" and either combine with each other on the slide, or grow in diameter. In an attempt to minimize the degree of water absorption by deposited particles during this transition, the microscope was enclosed and flushed with 5% relative humidity air. However, when transferring the slides from the jet to the microscope enclosure there was still significant water adsorption from the ambient lab air. When the laboratory air had a relative humidity > 30%, imaging measurements revealed deviations from Eq. (1) > 40% and deviations on the order of 15% for dryer lab conditions. It should be noted that the absorbtion of water and growth of the particles did not occur until after the particles had deposited on the microscope slide and the microscope slide was removed from the jet apparatus. Hence, none of the absorbtion issues described above affected the particle trajectories or impact location on the slide. In light of the above, Eq. (1) was used to obtain d for all of the results presented herein.

To obtain images of the rings, the microscope slides were back-lit and imaged at 1x using a digital camera (Cannon Rebel T3i) with a 65 mm macro lens (Canon MP-E 65 mm). The diameter and thickness of the rings were then measured using these 1x images. Measurements obtained from both the 1x and 10x images were generated by importing the captured images into ImageJ (Schneider et al. 2012). The 1x ring images were measured by manually drawing a circle over the inner and outer diameter of the rings and obtaining a pixel measurement of the diameters, which were then converted to lengths via calibration images of a fine-scaled rule which was imaged at the same location as the microscope slide.

3. Results

Representative ring-shaped deposition patterns are presented in Fig. 3. This figure shows that the ring inner diameter, outer diameter, and, concomitantly, ring thickness (one-half the outer diameter minus the inner diameter), vary with particle diameter d. Visual observation of Fig. 3 shows that the inner diameter gets smaller as the particle diameter increases from 6.16 μm to 12.98 μm. At $d = 12.98$ μm, the inner diameter of the ring has decreased to zero, as the entire circular region is filled in. There are a few anomalies in Fig. 3 which warrant discussion. First, the blurred checkerboard pattern in the background of all four images is a result of the LED array which was used to back-light

the microscope slides for imaging; the checkerboard pattern is simply an out-of-focus image of this array. Second, in Fig. 3(b), and to a lesser extent Figs. 3(a) and 3(c) there is some dust contamination visible. These dust particles are the linear objects visible inside the ring in Fig. 3(b), and the large dark particles in Figs. 3 (a) and 3(c). In color images, it is clear that these are dust since it is easy to distinguish between the orange-brown fluorescein particles generated in this experiment and the ambient dust, however this distinction is lost when reproduced in grayscale. Third, in Fig. 3(a) there is a faint second ring inside the well-defined primary ring. This is the result of the particle distribution not being perfectly monodisperse and will be discussed in more detail in Section 4. Fourth, in Figs. 3(a)–(c) the top portion of the deposit appears darker than the bottom. We hypothesize this is due to a slight cant in the mounting of the slide, making the top ~ 20 μm further from the nozzle than the bottom. Finally, the regular "cell" pattern in the deposit in Fig. 3(d) is due to the flow straightener in the nozzle, as there are the same number of "cells" within the deposit as the number of straws used in the flow straightener.

The particle velocity, U, and aerosol diameter, d, were varied. In Fig. 4, the ring dimensions are plotted against the particle Stokes number typically used to characterize impactors (Hinds 1982; Marple and Willeke 1976; Liu 1975):

$$Stk = \frac{\rho d^2 U}{9\mu W} \qquad (2)$$

where μ is the dynamic viscosity of air. These plots show the result of 182 deposition rings, binned in Stk, with bin widths of 0.03. The error bars show 95% confidence intervals for the ring dimension. As Fig. 4(a) shows, the inner diameter of the ring is very sensitive to Stk, varying from 15 mm to zero as Stk increases from 0.05 to 0.49. The ring outer diameter is relatively insensitive to Stk, decreasing from ~ 15 mm to slightly more than 12 mm over the same range of Stk. It is noted that no deposition was observed below $Stk \sim 0.035$, and at $Stk \sim 0.4$ the inner diameter approaches zero and is equal to zero at the largest Stk explored giving a ring thickness of $W/2$. This condition corresponds to a uniform deposition, which would be expected for a traditional impactor. Also of note, for a circular nozzle with $S/W > 1$, d_{50} will occur at $Stk_{50} = 0.24$ (Hinds 1982), and 100% collection of particles occurs at slightly higher Stk. Interestingly, this 100% collection would correspond approximately to the point in Stk space where the observed depositions from the small S/W impactor tested herein cease to be rings, and become uniform.
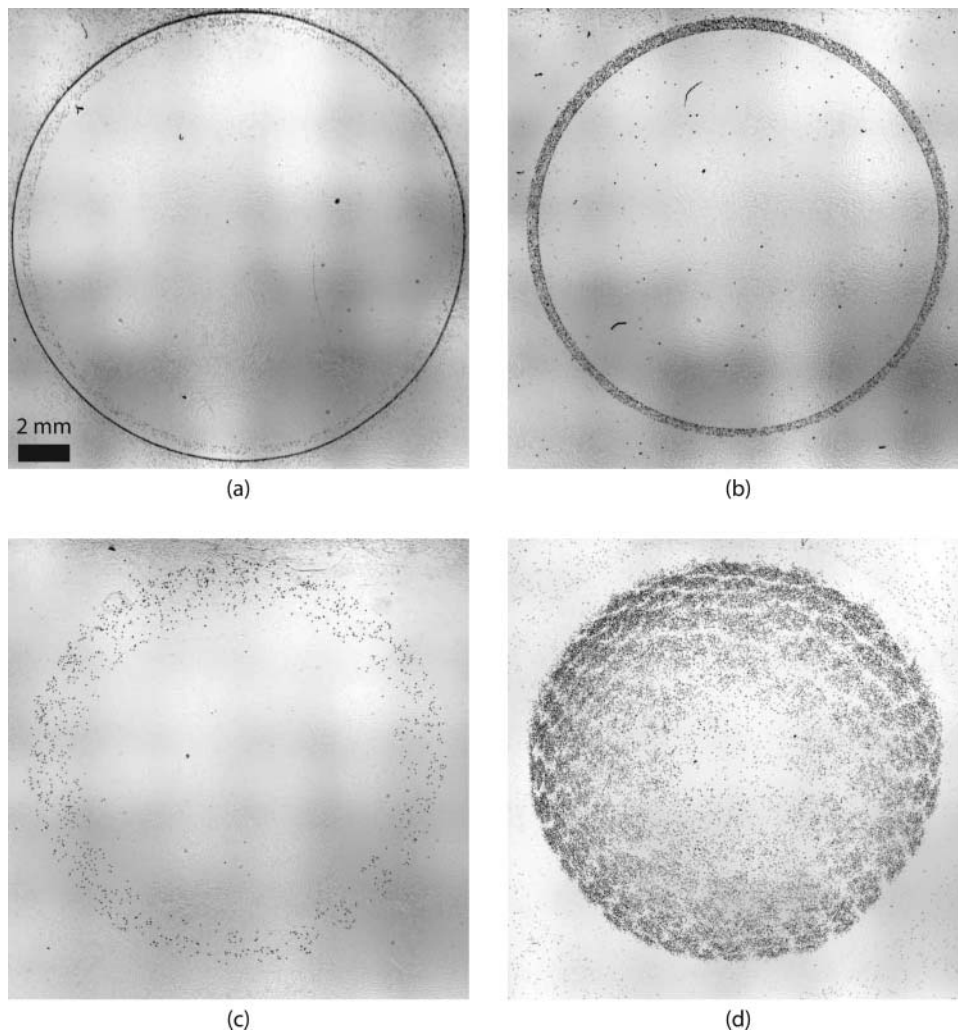
Figure 3. Representative particle deposition patterns imaged at 1x magnification for various particle diameters and jet velocities: (a) $d = 6.16$ μm, $Stk = 0.07$; (b) $d = 7.18$ μm, $Stk = 0.12$; (c) $d = 12.69$ μm, $Stk = 0.20$; (d) $d = 12.98$ μm, $Stk = 0.38$.

To investigate the influence of S/W on the ring dimensions, additional data was gathered at smaller S/W. This data is presented in Figs. S1 and S2 in the online supplemental information, and shows that the ring internal and external diameters increase with S/W.

The ring thickness is essentially unaffected by variation in S/W for the data collected.

To ensure that the rings formed during these experiments were truly a function of particle diameter, and not caused by some unknown process varying from
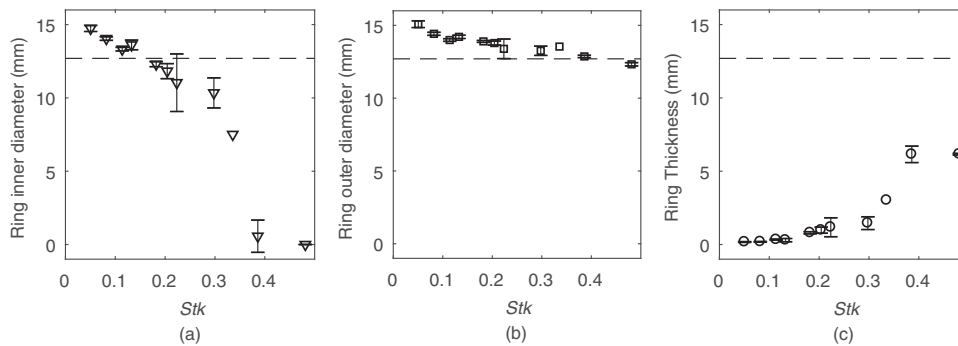

Figure 4. Relationship between ring dimensions and Stk: (a) Ring inner diameter versus Stk; (b) ring outer diameter versus Stk; (c) ring thickness versus Stk. The nozzle diameter, W, is shown as the dashed line.

experiment-to-experiment, rings were obtained for the case where two particle diameters were present in the jet at the same time. This was done by slightly detuning the VOAG to produce a bimodal aerosol. The existence of a bimodal distribution of drops leaving the VOAG is easily confirmed by providing a slight horizontal air flow over the VOAG head which, when illuminated from the side, shows two separated jets instead of one when the system is appropriately detuned. Running the VOAG in this detuned condition produced two different particle diameters as shown in Fig. 5. The bottom images in Fig. 5 show the 1x images of the deposition pattern resulting from the bimodal aerosol, revealing two well-defined rings, separated by a particle-free gap. The top images in this figure show a 10x view of the deposit, clearly showing that the larger diameter particles are located in the inner ring and the small particles in the outer ring, in agreement with the results presented in Figs. 3 and 4. Of note, some of the particles have soft, fluid-like edges and some appear to be in the process of merging, this is likely due to the hygroscopicity of the fluorescein particles discussed in Section 2. The possibility of particle merging prior to acquisition of the images presented in the images in Fig. 5 does not invalidate our conclusions, however, since this occurs once the particle has been deposited and therefore could not have influenced the particle's trajectory as it traveled from the nozzle to the slide.

4. Discussion

The deposition patterns on impactor plates for traditional impactors have been previously investigated and described in the literature. These investigations have found that for typical operating conditions, the deposition pattern of a polydisperse aerosol is nominally a Gaussian distribution centered on the nozzle axis (Rocklage et al. 2013; Roeber 1957; Berner 1978; Sethi and John 1993; John et al. 1991). These studies did not, however, investigate the size distributions within the particle deposits. Studies of monodisperse particles have shown that there is some correlation between the spatial distribution of deposited particles and particle diameter for particles near d_{50}, with larger particles tending to deposit closer to the centerline of the jet, and smaller particles migrating outward (Sethi and John 1993; John et al. 1991). However, this behavior appears to be the result of aerosol focusing in the impactor nozzle. Aerosol focusing will preferentially concentrate selected diameter particles
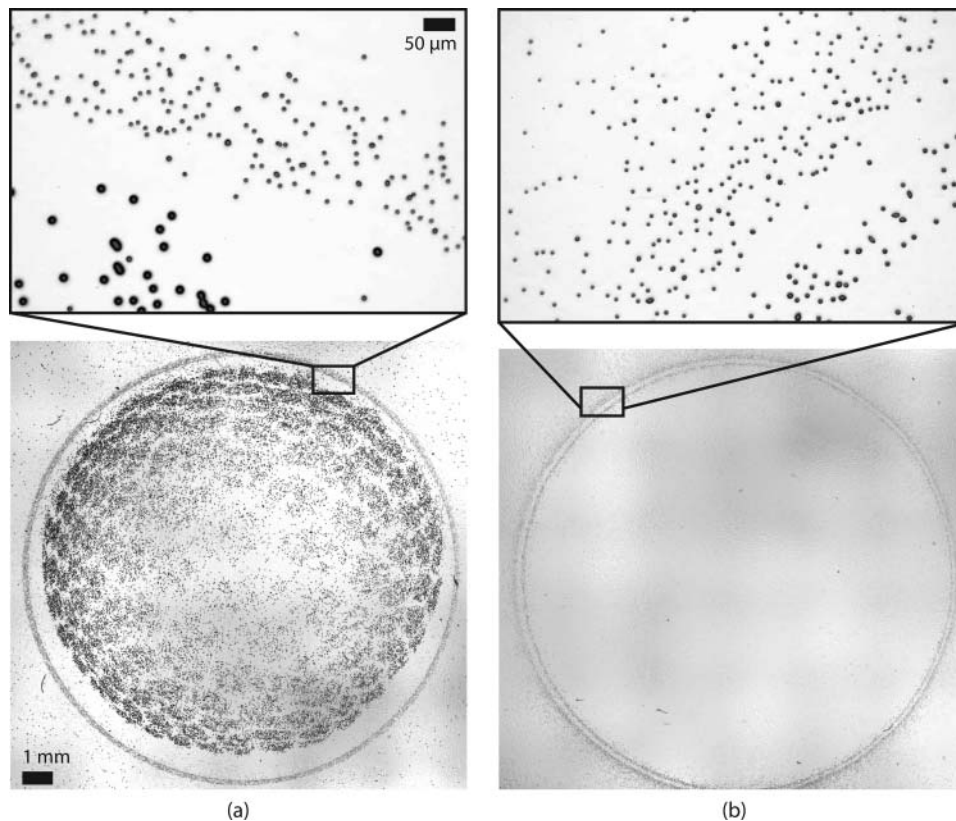
Figure 5. Deposition rings produced by bimodal particle distributions. The bottom images show two distinct deposition rings, separated by a thin particle-free region. The top images show magnified regions of the deposition rings, showing the size segregation of the deposited particles. The inner and outer deposition rings contain particles with d of (a) 12.98 μm and 7.9 μm and (b) 5.54 μm and 4.4 μm, respectively. This corresponds to Stk of (a) 0.40 and 0.14; and (b) 0.06 and 0.04, respectively.

to the centerline of the flow, the selected particle size being a function of the flow conditions and the nozzle geometry (Dahneke and Flachsbart 1972; Cheng and Dahneke 1979; Dahneke et al. 1982; Rao et al. 1993; Vidal-de Miguel and de la Mora 2012; Rennecke and Weber 2013). Burwash et al. (2006) found a similar deposition pattern with fixed particle sizes for high Reynolds number jets, and that the relationship between the deposition location was correlated with S/W. However, it should be noted that none of the above studies reveal a clear separation between particle deposition locations based on size, showing only a gradual shift in the radial extent of a Gaussian pattern.

In addition to the deposition patterns discussed above, secondary deposits, or "halos", have been occasionally observed ringing the main deposit on an impactor stage (Berner 1978; Roeber 1957; Rocklage et al. 2013; Oodo et al. 1981). The particles in these "halo" deposits have diameters smaller than d_{50} for the impaction stage, suggesting some relationship between deposition location and particle diameter, at least for particles smaller than d_{50}. However, we are unaware of any studies which explored whether and to what extent particles were geometrically segregated in these halos according to their size. Several mechanisms have been proposed to explain the formation of these "halo" deposits, including gravitational settling, Magnus lift, Saffman lift, and particle resuspension. However, we are unaware of any studies which examine the role of these proposed mechanisms in the formation of "halo" deposits on a diameter-resolved basis. All of these deposition patterns appear to be significantly different from those presented in the present work, as the observed rings, such as those presented in Figs. 3 and 5, are very well-defined with minimal blurring around the edges compared with those described in the literature above. Hence, the results presented herein showing a clear ring pattern for a monodisperse aerosol, where the ring diameter is clearly related to the particle diameter, is a new result.

It is worth noting that an instrument does exist which uses deposition location to size particles. This instrument is the inertial spectrometer, which relates aerosol diameter to the location along a curved path, where the aerosol is deposited (Prodi et al. 1979; Belosi and Prodi 1987). Obviously the flow conditions in this instrument are significantly different from those which exist in the impactor described in the present work.

The excellent correlation of the ring diameters with Stk shown in Fig. 4 suggests that the observed ring deposition patterns are governed by particle inertia. To help confirm this, an order of magnitude analysis is now presented to determine the degree of influence
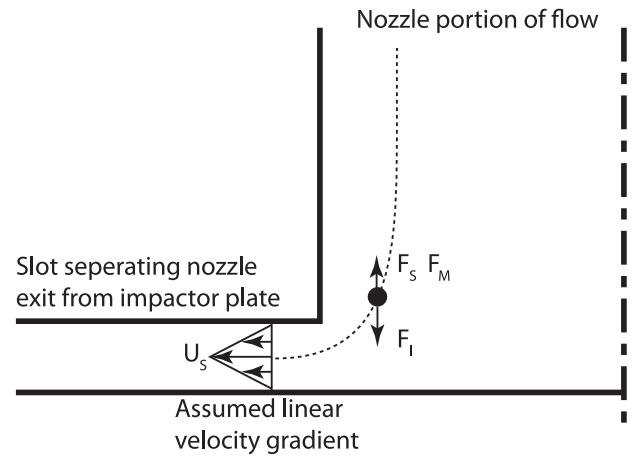

Figure 6. Free-body diagram of forces acting on the particle in a curvilinear path transitioning from the flow through the nozzle to flow through the slot gap between the nozzle exterior and the impactor slide. Also shown is the assumed velocity profile in the slot for the purpose of this order of magnitude analysis.

that other processes, such as Saffman lift, Magnus lift, and diffusion due to Brownian motion, as well as inertia, would have on the deposition patterns. A free body diagram is presented in Fig. 6 showing the forces considered as well as the assumed velocity profile within the slot separating the exterior of the nozzle (the region "F" shown in Fig. 2) and the impactor plate. All the forces considered are assumed to occur within the indicated slot.

The particle inertia was estimated using the acceleration required to stop a particle traveling at velocity U over a duration, τ; where τ is the relaxation time of the particle given by:

$$\tau = \frac{W \cdot Stk}{2U} \tag{3}$$

The particle inertial force, F_I, was then estimated as:

$$F_I = \frac{\rho \pi d^3 U}{6\tau} \tag{4}$$

The Saffman lift force, F_S, on a particle traveling through a velocity gradient, was estimated according to the work of Saffman (Saffman 1965, 1968) as:

$$F_S = 1.615 \rho_f d^2 U_S \sqrt{\nu \frac{dU_s}{dy}} \tag{5}$$

where ρ_f is the fluid density, ν is the kinematic viscosity, and U_S is the velocity through the slot. As indicated in Fig. 6, it was assumed that the velocity gradient in the slot was linear, and that there were no compressibility effects.

Table 1. Results of order of magnitude analysis of the influence that several mechanisms have on particles traveling through the gap between the nozzle and microscope slide for the conditions of the experiments presented herein.

Stk	d (μm)	U (m/s)	F_I (N)	F_S (N)	F_M (N)	δ_B (mm)
0.12	10	1.5	2.6×10^{-9}	1.4×10^{-9}	9.7×10^{-11}	1.8×10^{-4}
1.2×10^{-3}	1	1.5	2.6×10^{-10}	1.4×10^{-11}	9.7×10^{-14}	6.1×10^{-4}

The lift due to the rotation of a sphere, the Magnus effect, F_M, was obtained using the work of Rubinow and Keller (1961):

$$F_M = \frac{\pi}{8} d^3 \omega \rho_f U_S \qquad (6)$$

where ω is the angular velocity of the rotating particle. The rotation of the particle was estimated as a solid body rotation driven by the velocity difference across the particle.

Values of F_I, F_S, and F_M are presented in Table 1 for a range of conditions and particle diameters investigated in this work. These numbers show that inertia is the dominant force acting on the particles, except perhaps at large Stk where F_I is indeed larger than F_S, but only double its magnitude. Further investigation is needed, but it seems likely that inertia is the governing factor in the formation of these rings.

Finally, it is now demonstrated that the amount of "blurring" in the rings caused by Brownian motion of the particles is small compared to the measured ring dimensions. The particle drift, δ_B, due to Brownian motion was estimated as (Hinds 1982):

$$\delta_B = \sqrt{2Dt} \qquad (7)$$

where t is the transit time of a particle on the centerline to completely pass through the curved portion of the flow between the nozzle and the impaction plate, and D is the particle diffusivity defined as (Hinds 1982):

$$D = \frac{kTC_c}{3\pi\mu d} \qquad (8)$$

where k is the Boltzmann constant, C_c is the Cunningham slip correction, and T is the temperature. As Table 1 shows, the particles will move less than a micron due to diffusion, which is orders of magnitude smaller than the millimeter scale thickness of the rings presented here, and indicates that diffusion should be negligible in the formation of the observed rings.

5. Conclusion

Experiments were conducted to measure the deposition patterns resulting from an impactor with $S/W = 0.047$. The resulting deposition patterns were in the form of rings whose inner and outer diameter were correlated to Stk. These rings appear to be distinct from the impactor deposition patterns described by previous investigators. An order of magnitude analysis has shown that inertia is dominant for the particle sizes investigated and the most likely cause of the ring-shaped depositions observed. As the ring geometry is so well correlated with Stk, it may be possible to use the spatial location of deposition to help determine inter-stage particle size distributions if the results presented herein can be applied in a traditional impactor cascade.

References

Arffman, A., Marjamäki, M., and Keskinen, J. (2011). Simulation of Low Pressure Impactor Collection Efficiency Curves. *J. Aerosol Sci.*, 42(5):329–340.

Bell, J. H., and Mehta, R. D. (1988). Contraction design for small low-speed wind tunnels. Technical report, NASA.

Belosi, F., and Prodi, V. (1987). Particle Deposition within the Inertial Spectrometer. *J. Aerosol Sci.*, 18(1):37–42.

Berglund, R. N., and Liu, R. Y. H. (1973). Generation of Monodisperse Aerosol Standards. *Environ. Sci. Tech.*, 7:147–153.

Berner, A. (1978). Zur ursache sekundärer partikelniederschläge bei impaktoren. *Staub Reinhalt. Luft*, 38(1):1.

Burwash, W., Finlay, W., and Matida, E. (2006). Deposition of Particles by a Confined Impinging Jet onto a Flat Surface at Re=10^4. *Aerosol Sci. Technol.*, 40(3):147–156.

Chen, S. C., Tsai, C. J., Chen, H. D., Huang, C. Y., and Roam, G. D. (2011). The Influence of Relative Humidity on Nanoparticle Concentration and Particle Mass Distribution Measurements by the MOUDI. *Aerosol Sci. Technol.*, 45(5):596–603.

Cheng, Y. S., and Dahneke, B. E. (1979). Properties of Continuum Source Particle Beams: II. Beams Generated in Capillary Expansions. *J. Aerosol Sci.*, 10(4):363–368.

Dahneke, B., and Flachsbart, H. (1972). An Aerosol Beam Spectrometer. *J. Aerosol Sci.*, 3(5):345–349.

Dahneke, B., Hoover, J., and Cheng, Y. S. (1982). Similarity Theory for Aerosol Beams. *J. Colloid Interface Sci.*, 87(1):167–179.

Davis, D. L., Bell, M. L., and Fletcher, T. A. (2002). A Look Back at the London Smog of 1952 and the Half Century since. *Environ. Health Perspect.*, 110:A734–A735.

Docker, D. W., and Pope, C. A. (1994). Acute Respiratory Effects of Particulate Air Pollution. *Annu. Rev. Public Health*, 15:107–132.

Grinshpun, S. A., Mainelis, G., Trunov, M., Górny, R. L., Sivasubramani, S. K., Adhikari, A., and Reponen, T. (2005). Collection of Airborne Spores by Circular Single-Stage Impactors with Small Jet-to-Plate Distance. *J. Aerosol Sci.*, 36(5):575–591.

Hinds, W. C. (1982). *Aerosol Technology: Properties, Behavior, and Measurement of Airborne Particles*. New York, NY: Wiley-Interscience.

Horvath, H. (1993). Atmospheric Light Absorption: A Review. *Atmos. Environ. A-Gen.*, 27:293–317.

John, W., Fritter, D. N., and Winklmayr, W. (1991). Resuspension Induced by Impacting Particles. *J. Aerosol Sci.*, 22(6): 723–736.

Kanakidou, M., Seinfeld, J. H., Pandis, S. N., Barnes, I., Dentener, F. J., Facchini, M. C., Van Dingenen, R., Ervens, B., Nenes, A., Nielsen, C. J., Swietlicki, E., Putaud, J. P., Balkanski, Y., Fuzzi, S., Horth, J., Moortgat, G. K., Winterhalter, R., Myhre, C. E. L., Tsigaridis, K., Vignati, E., Stephanou, E. G., and Wilson, J. (2005). Organic Aerosol and Global Climate Modelling: A Review. *Atmos. Chem. Phys*, 5:1053–1123.

Liu, B. Y. H. (1975). *Fine Particles: Aerosol Generation, Measurement, Sampling, and Analysis*. New York: Academic Press Inc.

Marjamäki, M., Keskinen, J., Chen, D. R., and Pui, D. Y. H. (2000). Performance Evaluation of the Electrical Low-Pressure Impactor (ELPI). *J. Aerosol Sci.*, 31(2):249–261.

Marple, V. A. (2004). History of Impactors: The First 110 Years. *Aerosol Sci. Technol.*, 38(3):247–292.

Marple, V. A., Liu, B. Y. H., and Whitby, K. T. (1974). Fluid Mechanics of the Laminar Flow Aerosol Impactor. *J. Aerosol Sci.*, 5(1):1–16.

Marple, V. A., Rubow, K. L., and Behm, S. M. (1991). A Microorifice Uniform Deposit Impactor (MOUDI): Description, Calibration, and Use. *Aerosol Sci. Technol.*, 14(4):434–446.

Marple, V. A., and Willeke, K. (1976). Impactor Design. *Atmos. Environ.*, 10:891–896.

Oodo, T., Takashima, Y., and Hanzawa, M. (1981). An Experimental Study of Adhesion of Particles with a Round Nozzle Impactor. *J. Chem. Eng. Jpn.*, 14(1):76–78.

Pak, S. S., Liu, B. Y. H., and Rubow, K. L. (1992). Effect of Coating Thickness on Particle Bounce in Inertial Impactors. *Aerosol Sci. Technol.*, 16(3):141–150.

Pope, C. A., Thun, M. J., Namboodiri, M. M., Dockery, D. W., Evans, J. S., Speizer, F. E., and Heath, C. W. (1995). Particulate Air Pollution as a Predictor of Mortality in a Prospective Study of U.S. Adults. *Am. J. Respir. Crit. Care Med.*, 151:669–674.

Prodi, V., Melandri, C., Tarroni, G., De Zaiacomo, T., Formignani, M., and Hochrainer, D. (1979). An Inertial Spectrometer for Aerosol Particles. *J. Aerosol Sci.*, 10(4): 411–419.

Pruppacher, H., and Klett, J. (1978). *Microphysics of Clouds and Precipitation*. Dordrecht: Reidel.

Ramanathan, V., Crutzen, P. J., Kiehl, J. T., and Rosenfeld, D. (2001). Aerosols, Climate, and the Hydrological Cycle. *Science*, 294:2119–2124.

Rao, N. P., Navascues, J., and De La Mora, J. F. (1993). Aerodynamic Focusing of Particles in Viscous Jets. *J. Aerosol Sci.*, 24(7):879–892.

Rennecke, S., and Weber, A. P. (2013). A Novel Model for the Determination of Nanoparticle Impact Velocity in Low Pressure Impactors. *J. Aerosol Sci.*, 55:89–103.

Rocklage, J. M., Marple, V. A., and Olson, B. A. (2013). Study of Secondary Deposits in Multiple Round Nozzle Impactors. *Aerosol Sci. Technol.*, 47(10):1144–1151.

Roeber, R. (1957). Untersuchungen zur konimetrischen staubmessung. *Staub*, 49:273–295.

Rubinow, S. I., and Keller, J. B. (1961). The Transverse Force on a Spinning Sphere Moving in a Viscous Fluid. *J. Fluid Mech.*, 11(3):447–459.

Saffman, P. G. T. (1965). The Lift on a Small Sphere in a Slow Shear Flow. *J. Fluid Mech.*, 22(02):385–400.

Saffman, P. G. T. (1968). The Lift on a Small Sphere in a Slow Shear Flow: Corrigendum. *J. Fluid Mech.*, 31:624.

Schneider, C. A., Rasband, W. S., and Eliceiri, K. W. (2012). NIH Image to ImageJ: 25 years of Image Analysis. *Nat. Methods*, 9(7):671.

Schwartz, J. (1994). What are People Dying of on High Air Pollution Days? *Environ. Res.*, 64:26–35.

Schwartz, J., and Dockery, D. W. (1992). Increased Mortality in Philadelphia Associated with Daily Air Pollution Concentrations. *Am. Rev. Respir. Dis.*, 145:600–604.

Schwartz, J., Laden, F., and Zanobetti, A. (2002). The Concentration–Response Relation between PM2.5 and Daily Deaths. *Environ. Health Perspect.*, 110(10):1025–1029.

Seaton, A., MacNee, W., Donaldson, K., and Godden, D. (1995). Particulate Air Pollution and Acute Health Effects. *The Lancet*, 345:176–178.

Sethi, V., and John, W. (1993). Particle Impaction Patterns from a Circular Jet. *Aerosol Sci. Technol.*, 18(1):1–10.

Tsai, C. J., Liu, C. N., Hung, S. M., Chen, S. C., Uang, S. N., Cheng, Y. S., and Zhou, Y. (2012). Novel Active Personal Nanoparticle Sampler for the Exposure Assessment of Nanoparticles in Workplaces. *Environ. Sci. Technol.*, 46 (8):4546–4552.

Turner, J. R., and Hering, S. V. (1987). Greased and Oiled Substrates as Bounce-Free Impaction Surfaces. *J. Aerosol Sci.*, 18(2):215–224.

Vidal-de Miguel, G., and de la Mora, J. F. (2012). Continuously Converging Multistage Focusing Lenses to Concentrate Aerosols at High Reynolds Numbers. *Aerosol Sci. Technol.*, 46(3):287–296.

Vincent, J. H. (2007). *Aerosol Sampling: Science, Standards, Instrumentation and Applications*. London: John Wiley & Sons.